Atmos. Chem. Phys. Discuss., 15, 12167–12212, 2015
www.atmos-chem-phys-discuss.net/15/12167/2015/
doi:10.5194/acpd-15-12167-2015

Atmospheric Chemistry and Physics Discussions

Estimating collision efficiencies from contact freezing experiments

B. Nagare[1], C. Marcolli[1,2], O. Stetzer[1], and U. Lohmann[1]

[1]Institute for Atmospheric and Climate Science, ETH, Zurich Switzerland
[2]Marcolli Chemistry and Physics Consulting GmbH, Zurich, Switzerland

Received: 19 March 2015 – Accepted: 3 April 2015 – Published: 23 April 2015

Correspondence to: C. Marcolli (claudia.marcolli@env.ethz.ch)

Published by Copernicus Publications on behalf of the European Geosciences Union.

Abstract

Interactions of atmospheric aerosols with clouds influence cloud properties and modify the aerosol life cycle. Aerosol particles act as cloud condensation nuclei and ice nucleating particles or become incorporated into cloud droplets by scavenging. For an accurate description of aerosol scavenging and ice nucleation in contact mode, collision efficiency between droplets and aerosol particles needs to be known. This study derives the collision rate from experimental contact freezing data obtained with the ETH Collision Ice Nucleation Chamber CLINCH. Freely falling 80 µm water droplets are exposed to an aerosol consisting of 200 nm diameter silver iodide particles of concentrations from 500–5000 cm^{-3}, which act as ice nucleating particles in contact mode. The chamber is kept at ice saturation in the temperature range from 236–261 K leading to slow evaporation of water droplets giving rise to thermophoresis and diffusiophoresis. Droplets and particles bear charges inducing electrophoresis. The experimentally derived collision efficiency of 0.13 is around one order of magnitude higher than theoretical formulations which include Brownian diffusion, impaction, interception, thermophoretic, diffusiophoretic and electric forces. This discrepancy is most probably due to uncertainties and inaccuracies in the description of thermophoretic and diffusiophoretic processes acting together. This is to the authors knowledge the first dataset of collision efficiencies acquired below 273 K. More such experiments with different droplet and particle diameters are needed to improve our understanding of collision processes acting together.

1 Introduction

Interactions of atmospheric aerosols with clouds influence the cloud properties and modify the aerosol life cycle. Depending on particle size, morphology and chemical composition, aerosol particles act as cloud condensation nuclei (CCN) and ice nucleating particles (INP) or become incorporated into cloud droplets by scavenging. Scav-

ACPD
15, 12167–12212, 2015

enging of particles in the air is one of the major processes by which the atmosphere is cleansed (Radke et al., 1980). Particles may be scavenged in-cloud and below-cloud due to collision with droplets (impaction scavenging) or by nucleation scavenging when they serve as CCN or INP (Leong et al., 1982). Below 273 K solid aerosol particles that activate to cloud droplets may induce droplet freezing in immersion mode when the temperature is further decreased. This freezing process is usually discriminated from condensation freezing, where CCN activation is immediately followed by ice formation. When interstitial aerosol particles collide with cloud droplets they may induce freezing in contact mode. This nucleation process deserves special attention, since it is reported to induce ice nucleation at higher temperature than when the same particle acts as INP in immersion or condensation mode (Durant and Shaw, 2005; Fornea et al., 2009; Ladino Moreno et al., 2013). In addition, the importance of contact nucleation for cloud glaciation also depends on the collision efficiency between aerosol and cloud droplets.

Collisions between particles and droplets can result from motion induced by turbulence and Brownian diffusion or as a result of external forces induced by gravity, electric charges, temperature or vapor gradients (Leong et al., 1982). There exist different formulations that describe collision efficiencies theoretically and give mathematical expressions for them (Slinn, 1983; Park et al., 2005; Andronache et al., 2006; Wang and Pruppacher, 1977). To validate theoretical calculations, laboratory studies have been carried out in which aerosols have been exposed to falling droplets (see Wang et al., 1978 and Ladino et al., 2011b for references). Most of these studies have been performed at or close to room temperature with droplets of sizes that are typical for drizzle and rain drops rather than for cloud droplets. Measurements of pre- and post-rain aerosol concentrations have been used to quantify aerosol scavenging by precipitation (Davenport and Peters, 1978; Laakso et al., 2003; Chate and Pranesha, 2004; Maria and Russell, 2005). These studies often show too large washout compared with theoretical estimates based on formulations of collision efficiencies (Andronache et al., 2006). One reason for this might be an inaccurate representation of the collision pro-

ACPD
15, 12167–12212, 2015

cesses. Accurate estimates of collision efficiencies are also needed to describe cloud glaciation. Up to date, there is lack of atmospheric INP that might explain ice nucleation at temperatures higher than −15 °C. While biological particles are discussed as candidates to close this gap (DeMott et al., 2010), an alternative explanation would be ice nucleation in contact mode. Several field studies have observed that ice crystals preferentially formed in regions of downdrafts and at cloud edges where dry air is entrained (Young, 1974). Particles contained in these air masses could initiate droplet freezing when they collide with them. To judge the importance of this process nucleation and collision efficiencies have to be quantified. The representation of heterogeneous ice nucleation in most global models still lacks a detailed description of the freezing processes depending on aerosol properties and nucleation mode (Yun and Penner, 2012; Lohmann and Hoose, 2009).

Depending on particle size and the forces acting on the particles, different collision processes have to be taken into account. In models, collision efficiencies are usually calculated as the sum of the different collision processes (Andronache et al., 2006; Bae et al., 2009; Croft et al., 2010) neglecting that the forces act together to determine the aerosol path either into or around the droplet. Trajectory calculations can be used to simulate the particle pathway, however, they need to be validated with reliable laboratory measurements (Tinsley and Leddon, 2013). Calculated collision efficiencies are quite accurate for Aitken and coarse mode particles, for which either Brownian diffusion or impaction dominates. Accumulation mode particles fall into the particle size range of the Greenfield gap (Greenfield, 1957; Seinfeld and Pandis, 2006; Ladino et al., 2011a), where Brownian diffusion and impaction are inefficient collision mechanisms. However, the collision efficiency minimum of the Greenfield gap is reduced in the presence of electric or phoretic forces and theoretical descriptions have to include the corresponding contributions to the collision efficiencies to give accurate values. Only few experimental studies have explored this part of the parameter space (Ladino et al., 2011a; Ladino, 2011) and none of them at mixed-phase cloud temperatures.

ACPD
15, 12167–12212, 2015

The present study investigates collision efficiency of 200 nm diameter silver iodide (AgI) particles with 80 µm droplets at low temperatures. Droplets and particles bear charges giving rise to electric forces and droplets are slowly evaporating inducing thermophoretic and diffusiophoretic forces. This study therefore provides experimental data to validate theoretical formulations exactly in this least explored parameter space range. The paper is structured as follows: Sect. 2 presents theoretical formulations of collision efficiencies from the literature, Sects. 3 and 4 describe the experimental procedure and the results. In Sects. 5 and 6, the theoretical formulations are compared with experimental results and are critically discussed. Comparison with other experimental work is presented in Sect. 6. Section 7 discusses improvements of theoretical formulations and atmospheric implications.

2 Theory

2.1 Collision efficiency

When a droplet falls through air, various processes can lead to the collision of aerosol particles with droplets. Theoretical formulations of these processes generally assume a flow around a spherical droplet capturing spherical particles. The collision efficiency (E) is defined as the fraction of particles in the cylindrical volume swept out by a falling droplet that collide with the droplet. A collision efficiency of unity is realized when all the particles residing in the swept out volume of a droplet collide with the droplet. When the particles follow the air stream around the droplet, E is smaller than one. E can exceed unity when particles get scavenged by wake capture. The coalescence efficiency is defined as the fraction of particles that are retained by the droplet when they collide with them. The product of E and coalescence is called the collection efficiency. Normally, it is assumed that a collision leads to the scavenging of the particle by the droplet so that the collision efficiency and collection efficiency are the same. Different processes have to be considered that cause deviations of the particle's movement from the air stream

ACPD
15, 12167–12212, 2015

path and lead to the collision of aerosols with droplets (Ladino et al., 2011b). For the smallest particles, Brownian diffusion is the most important collision process. Brownian diffusion describes the random motion of aerosol particles resulting from collisions with carrier gas molecules. It is a strong function of particle size being most important for small aerosol particles. Large particles are most efficiently scavenged by inertial interception and impaction. Inertial impaction occurs when a particle is unable to follow the streamlines around a falling droplet and, because of its inertia, continues to move toward the drop and is eventually captured by it (Seinfeld and Pandis, 2006). Interception takes place when a particle follows the streamlines around a falling droplet sufficiently close to collide with it. The region of low collision efficiency between the small and large aerosol particles is known as the Greenfield gap. This gap may at least be partly closed when electric and phoretic effects contribute to particle collisions. Thermophoresis describes a net transport of particles in the presence of a temperature gradient in the air. Air molecules at higher temperature have a higher mean velocity and therefore impart more momentum on a particle than colder ones. The momentum on the warmer side of the particle is therefore larger and moves particles from higher to lower temperatures. Since evaporation cools the droplets and induces a temperature gradient in the surrounding air, particles are attracted by droplets for RH < 100 % because of thermophoresis. Diffusiophoresis arises in the presence of a vapor concentration gradient. In the case of an evaporating droplet, there is a flux of water molecules away from the droplet, compensated by a flux of carrier gas molecules (mainly N_2, O_2) in the opposite direction (Stephan flow) to keep the total pressure constant. These flows exert a repulsive force on the particle. Under typical atmospheric conditions thermophoresis dominates diffusiophoresis for aerosol particles < 1 µm (Slinn and Hales, 1971). Finally, in case of charged particles and droplets, electroscavenging has to be considered as an additional collision process. Usually, collision efficiencies of each of these processes are formulated separately and added together to yield the total collision efficiency E_{tot}. Park et al. (2005) and Slinn (1983) proposed formulations for the collision efficiencies by Brownian diffusion (E_{Br}), interception (E_{int}), and impaction (E_{imp}). Andronache

ACPD
15, 12167–12212, 2015

et al. (2006) gives formulations for thermophoresis (E_{Th}), diffusiophoresis (E_{Df}), and electrophoresis (E_{El}). Wang et al. (1978) use a flux model to calculate collision rate coefficients for electric and phoretic scavenging. In the following, we will outline the formulations proposed for the different collision processes.

2.2 Brownian diffusion, interception and impaction

In the approaches by Park et al. (2005), hereafter referred to as P05, and Slinn (1983), hereafter referred to as S83, collision efficiencies of Brownian diffusion, interception and impaction ($E_{Br,I}$) are provided. They are calculated separately and added together.

$$E_{Br,I} = E_{Br} + E_{int} + E_{imp} \tag{1}$$

2.2.1 Formulation by Park (P05)

For collision efficiencies due to Brownian diffusion and interception Park et al. (2005) follow Jung and Lee (1998) who used a resolved flow field around a system consisting of multiple spheres to obtain an analytical solution including the effects of induced internal circulation inside a liquid droplet. Due to the influence of the internal flow, the outer flow velocity around the fluid spheres becomes larger than that around solid spheres. For this reason, the streamlines pass around a fluid sphere more closely than around a solid sphere. The collision efficiency due to Brownian diffusion is taken from Park et al. (2005):

$$E_{Br}(d_p, D_d) = 2\left(\frac{\sqrt{3}\pi}{4P_e}\right)^{\frac{2}{3}}\left(\frac{(1-\alpha)(3\sigma+4)}{(J+\sigma K)}\right)^{\frac{1}{3}} \tag{2}$$

ACPD
15, 12167–12212, 2015

where α is the packing density i.e. the water volume present in a unit volume of air and σ the viscosity ratio of water to air. The hydrodynamic factors J and K are given as

$$J = 1 - \frac{6}{5}\alpha^{\frac{1}{3}} + \frac{1}{5}\alpha^2$$

$$K = 1 - \frac{9}{5}\alpha^{\frac{1}{3}} + \alpha + \frac{1}{5}\alpha^2$$

and P_e is the Peclet number defined as the ratio between the advective and diffusive transport rate and is given as

$$P_e = \frac{D_d U(D_d)}{D_{diff}}$$

where D_d is the droplet diameter, $U(D_d)$ is the terminal velocity of the drop and D_{diff} the diffusion coefficient of aerosol particles given by

$$D_{diff} = \frac{k_B T_a \, C_c(d_p)}{3\pi\mu_a \, d_p}$$

where k_B is the Boltzmann constant, T_a is the air temperature in K, μ_a is the dynamic viscosity of air and $C_c(d_p)$ is the Cunningham slip correction factor to account for non-continuum effects associated with small particles. It is given as (Ladino et al., 2011a)

$$C_c(d_p) = 1 + \frac{2\lambda_a}{d_p}\left[1.257 + 0.4\exp\frac{-1.1 d_p}{2\lambda_a}\right]$$

where λ_a is the mean free path of air molecules. The temperature dependent viscosity of air μ_a is taken from the parametrization in Pruppacher and Klett (1997). In poise units it is given as

$$\mu_a = \frac{1.718 + 0.0049T_c - 0.000012T_c^2}{10^{-4}}$$

ACPD
15, 12167–12212, 2015

where T_c is the temperature in °C. For the viscosity of water the lowest measured value at 273 K is used ($1.787 \times 10^{-3}\,\mathrm{kg\,m^{-1}\,s^{-1}}$).

According to Jung and Lee (1998) the collision efficiency due to interception E_{int} is given as

$$E_{\mathrm{int}}(d_{\mathrm{p}}, D_{\mathrm{d}}) = \frac{1-\alpha}{J+\sigma K}\left[\frac{R}{1+R} + \frac{1}{2}\left(\frac{R}{1+R}\right)^2 (3\sigma+4)\right] \tag{3}$$

where R is the diameter ratio between particle and droplet $\frac{d_{\mathrm{p}}}{D_{\mathrm{d}}}$.

The collision efficiency due to impaction E_{imp} is given as

$$E_{\mathrm{imp}}(d_{\mathrm{p}}, D_{\mathrm{d}}) = \left(\frac{Stk}{Stk+0.35}\right)^2 \tag{4}$$

where Stk is the Stokes number

$$Stk = \frac{\rho_{\mathrm{p}} d_{\mathrm{p}}^2 U(D_{\mathrm{d}})}{18\mu_{\mathrm{a}}\, D_{\mathrm{d}}}$$

and ρ_{p} is the density of the particles.

2.2.2 Formulation by Slinn (S83)

Slinn (1983) proposed formulations for E_{Br}, E_{int} and E_{imp} using dimensional analysis coupled with experimental data which are summarized in Seinfeld and Pandis (2006). Based on Slinn (1983), the following formulations are given in Seinfeld and Pandis

ACPD
15, 12167–12212, 2015

(2006) and Wang et al. (2010)

$$E_{\mathrm{Br}}(d_{\mathrm{p}}, D_{\mathrm{d}}) = \frac{4}{ReSc}(1 + 0.4Re^{\frac{1}{2}}Sc^{\frac{1}{3}} + 0.16Re^{\frac{1}{2}}Sc^{\frac{1}{2}}) \quad (5)$$

$$E_{\mathrm{int}}(d_{\mathrm{p}}, D_{\mathrm{d}}) = 4\frac{d_{\mathrm{p}}}{D_{\mathrm{d}}}\left[\frac{\mu_{\mathrm{a}}}{\mu_w} + (1 + 2Re^{\frac{1}{2}})\frac{d_{\mathrm{p}}}{D_{\mathrm{d}}}\right] \quad (6)$$

$$E_{\mathrm{imp}}(d_{\mathrm{p}}, D_{\mathrm{d}}) = \left(\frac{\rho_{\mathrm{w}}}{\rho_{\mathrm{p}}}\right)^{\frac{1}{2}}\left(\frac{St - St^*}{St - St^* + \frac{2}{3}}\right)^{\frac{3}{2}} \quad (7)$$

where ρ_{w} and ρ_{p} are densities of liquid water and particles respectively. The normalizing factor $\frac{\rho_{\mathrm{w}}}{\rho_{\mathrm{p}}}$ is necessary to account for aerosol particles with density > 1000 kg m^{-3}. Re is the Reynolds number representing the ratio of inertial to viscous forces in the flow and given by Pruppacher and Klett (1997).

$$Re = \exp(Y)$$

where Y is

$$Y = -3.18657 + 0.992696X - 0.00153193X^2 - 0.000987059X^3 - 0.000578878X^4 + 0.000085517X^5 - 0.00000327815X^6$$

where $X = \ln(\mathrm{CdRe}^2)$ and CdRe^2 is given as

$$\mathrm{CdRe}^2 = \frac{4D_{\mathrm{d}}^3(\rho_{\mathrm{w}} - \rho_{\mathrm{a}})g}{3\mu_{\mathrm{a}}^2}$$

where ρ_{a} is the density of air, g is the acceleration due to gravity. Sc is the Schmidt number of aerosol particles, St is the particle Stokes number given as

$$St = \frac{2\tau(U(D_{\mathrm{d}}) - u(d_{\mathrm{p}}))}{D_{\mathrm{d}}}$$

ACPD
15, 12167–12212, 2015

$U(D_d)$ and $u(d_p)$ are the terminal velocities of the droplets and aerosol particles, respectively. The relaxation time τ is given as (Wang et al., 2010),

$$\tau = \frac{(\rho_p - \rho_a) d_p^2 C_c}{18 \mu_a}$$

St^* is the critical Stokes number above which particles may be deposited on the droplet. Note that S83 uses a slightly different formula for the Stokes number (St) than P05 (Stk). In the formulation for E_{imp} given in Eq. (7) collision can happen only when $St > St^*$. The critical Stokes number is given as

$$St^* = \frac{1.2 + \frac{1}{12}\ln(1 + Re)}{1 + \ln(1 + Re)}$$

2.3 Phoretic forces

Since inside the collision chamber, the droplets are evaporating, thermo- and diffusiophoretic forces also contribute to the collision efficiency. Electroscavenging has to be taken into account because particles and droplets are charged. We consider the formulations of Andronache (2004); Andronache et al. (2006), hereafter referred to as A06, where collision efficiencies are calculated separately and added together to obtain the total collision efficiency due to phoretic forces E_{ph}

$$E_{ph} = E_{Th} + E_{Df} + E_{El} \quad (8)$$

where E_{Th}, E_{Df} and E_{El} are the collision efficiencies due to thermophoresis, diffusiophoresis and electrophoresis, respectively.

ACPD
15, 12167–12212, 2015

2.3.1 Formulation by Andronache (A06)

The contribution of thermophoresis to the collision efficiency is given as (Andronache et al., 2006)

$$E_{\mathrm{Th}}(d_{\mathrm{p}}, D_{\mathrm{d}}) = \frac{4\gamma(2 + 0.6Re^{\frac{1}{2}}P_{\mathrm{r}}^{\frac{1}{3}})(T_{\mathrm{a}} - T_{\mathrm{s}})}{U(D_{\mathrm{d}})D_{\mathrm{d}}} \tag{9}$$

where T_{a} is the absolute temperature of air, T_{s} is the absolute temperature at the droplet surface and P_{r} the Prandtl number for air given as

$$P_{\mathrm{r}} = \frac{C_p \mu_{\mathrm{a}}}{k_{\mathrm{a}}}.$$

γ is given as

$$\gamma = \frac{2C_{\mathrm{c}}\left(k_{\mathrm{a}} + 5\frac{\lambda_{\mathrm{a}}}{D_{\mathrm{d}}}k_{\mathrm{p}}\right)k_{\mathrm{a}}}{5p\left(1 + 6\frac{\lambda_{\mathrm{a}}}{D_{\mathrm{d}}}\right)\left(2k_{\mathrm{a}} + k_{\mathrm{p}} + 10\frac{\lambda_{\mathrm{a}}}{D_{\mathrm{d}}}k_{\mathrm{p}}\right)}$$

where k_{a} and k_{p} are the thermal conductivities of the air and the aerosol particles, p is the atmospheric pressure and C_p is the specific heat of air at constant pressure. The diffusiophoretic contribution to collision efficiency is given as

$$E_{\mathrm{Df}}(d_{\mathrm{p}}, D_{\mathrm{d}}) = \frac{4\beta(2 + 0.6Re^{\frac{1}{2}}\mathrm{Sc}_{\mathrm{w}}^{\frac{1}{3}})(\frac{p_{\mathrm{s}}^0}{T_{\mathrm{s}}} - \frac{p_{\mathrm{a}}^0 \mathrm{RH}}{T_{\mathrm{a}}})}{U(D_{\mathrm{d}})D_{\mathrm{d}}} \tag{10}$$

where

$$\beta = \frac{T_{\mathrm{a}}D_{\mathrm{w}}}{p} \cdot \left(\frac{M_{\mathrm{w}}}{M_{\mathrm{a}}}\right)^{\frac{1}{2}}$$

ACPD
15, 12167–12212, 2015

The Schmidt number for water vapor in air is given as

$$\mathrm{Sc_w} = \frac{\mu_a}{\rho_a D_w}$$

where D_w is the diffusivity of water vapor in air. For evaporating droplets, the diffusiophoretic contribution to E is negative. In the formulation by Andronache et al. (2006), the contribution of electric charge to the scavenging efficiency is based on Coulomb interactions between aerosol particles and droplets carrying point charges of opposite sign, leading to the capture of particles present on the streamline close to the droplet surface. The expression for this electrostatic collision efficiency is given as (Andronache, 2004; Davenport and Peters, 1978)

$$E_{El}(d_p, D_d) = \frac{16 K C_c Q q}{3\pi\mu_a D_d^2 d_p U(D_d)} \quad (11)$$

where $K = 9 \times 10^9\,\mathrm{N\,m^2\,C^{-2}}$, Q and q are the mean charges on the droplet and the aerosol particle in Coulomb units.

2.3.2 The flux model (W78)

An alternative formulation for phoretic and electrostatic forces is given by the flux model (Wang et al., 1978), hereafter referred to as W78. It expresses the thermophoretic force F_{Th} as (Tinsley et al., 2006)

$$F_{Th} = -\frac{6\pi\mu_a d_p (k_a + 2.5 k_p Kn) k_a}{5(1+3Kn)(k_p + 2k_a + 5k_p Kn)p} \frac{2(T_a - T_s)}{D_d r^2} \quad (12)$$

where r is the distance between the center of the droplet and the particle and Kn the Knudsen number. The term $\frac{2(T_a - T_s)}{D_d r^2}$ is the temperature gradient between the absolute

ACPD
15, 12167–12212, 2015

temperature of the surrounding (T_a) and at the droplet surface (T_s), assuming spherical symmetry. The diffusiophoretic force can be expressed as (Tinsley et al., 2006)

$$F_{Df} = -\frac{3\pi\mu_a d_p(0.74)D_w M_a}{(1+\alpha Kn)M_w\rho_a}\frac{2(\rho_{v,a}-\rho_{v,s})}{D_d r^2} \quad (13)$$

The last term in this expression $\frac{2(\rho_{v,a}-\rho_{v,s})}{D_d r^2}$ is the gradient in water vapor density. M_a and M_w are the molecular weights of air and water, $\rho_{v,a}$ and $\rho_{v,s}$ are the water vapor densities in the air far from the droplet and at the droplet surface, respectively. The parameter α is given as (Wang et al., 1978)

$$\alpha = 1.26 + 0.40\exp(-1.10Kn^{-1})$$

The formulation of the forces is strictly valid only for spherically symmetric inverse square fields. This is the case for stationary droplets. If the droplet moves, the temperature and vapor fields are not spherically symmetric. As a first order correction, mean heat and vapor ventilation coefficients f_h and f_v, respectively, can be introduced to account for the effect of air motion on the flux of heat and water vapor (Tinsley, 2010). With this correction, the forces may be expressed as $F_{Th} = \frac{C_{Th}}{r^2 f_h}$ and $F_{Df} = \frac{C_{Df}}{r^2 f_v}$ where C_{Th} and C_{Df} are inverse square force constants for thermophoresis and diffusiophoresis, $C_{Th} = f_h F_{Th} r^2$ and $C_{Df} = f_v F_{Df} r^2$. The inverse square force constants C for the thermophoretic force and the diffusiophoretic force can be formulated as (Wang et al., 1978)

$$C_{Th} = -\frac{3\pi\mu_a d_p(k_a + 2.5k_p Kn)k_a\, D_d(T_a - T_s)f_h}{5(1+3Kn)(k_p+2k_a+5k_p Kn)p} \quad (14)$$

$$C_{Df} = -\frac{3}{2}\frac{\pi\mu_a\, D_d(0.74)D_w M_a\, d_p(\rho_{v,a}-\rho_{v,s})f_v}{(1+\alpha Kn)M_w\rho_a} \quad (15)$$

ACPD
15, 12167–12212, 2015

If electric forces are approximated by inverse square forces (repulsive for like charges, attractive for unlike charges and neglecting image charges), the inverse square force constant for electrical forces is (Tinsley, 2010)

$$C_{\mathrm{El}} = \frac{Qq}{4\pi\epsilon_0} \tag{16}$$

Using the relationship between collision efficiency and collision kernel, an effective collision efficiency can be derived from the forces. The collsion kernel K for each force constant C can be calculated as (Ladino et al., 2011b)

$$K = \frac{4\pi B_{\mathrm{p}} C}{\exp(\frac{2B_{\mathrm{p}}C}{D_{\mathrm{diff}} f_p d_{\mathrm{p}}}) - 1} \tag{17}$$

where B_{p} is the mobility of particles. From the collision kernel, the different collision efficiencies for each mechanism can be calculated using the relationship

$$E = \frac{4K}{\pi(D_{\mathrm{d}} + d_{\mathrm{p}})^2 (U(D_{\mathrm{d}}) - u(d_{\mathrm{p}}))}. \tag{18}$$

3 Experimental setup

3.1 Instrumentation

Our collision nucleation chamber (CLINCH) is similar to the one used by Ladino et al. (2011b) for contact freezing studies with some modifications to observe the frozen fraction of droplets at different times. It is a continuous flow chamber which consists of two parallel plates separated by 1 cm width with side windows for the detector. Both chamber walls are held at the same temperature and are covered with ice, leading to an environment that is saturated with respect to ice and subsaturated with respect to

ACPD
15, 12167–12212, 2015

water. Relative humidity in the chamber depends on the chamber temperature. The droplet generator from Bremen University is placed at the center top of the chamber. The droplet generator contains a piezo element which can produce 80 µm diameter droplets with a frequency of 100 droplets per second (Ulmke et al., 2001). With this setting the distance between two successive droplets is about 2 mm when the droplet acquires its terminal velocity of 0.182 m s^{-1}. The droplets are generated with pure water (Milli-Q, 18.2 MΩ) at a temperature of 281 K. The relaxation time for a droplet to reach its terminal velocity is 0.2 s and the temperature relaxation time is about 0.6 s when the chamber is kept at 235 K. Aerosol particles enter the chamber at the top in an air flow from both sides and can interact with the liquid droplets while passing through the chamber. The flow through the chamber is laminar and should not show any turbulence. The terminal velocity of the AgI aerosol is too low to contribute to the flow velocity. The fall velocity of the aerosol particles is therefore taken as the flow velocity averaged over the whole cross section of the chamber, which equals 0.017 m s^{-1} for an air flow of 1 liter per minute through the chamber. In CLINCH, aerosol particles and cloud droplets can collide leading to freezing of the cloud droplets via contact freezing. With the modified setup, it is possible to observe the frozen fraction of droplets at lengths of 40 and 80 cm. The residence time of droplets at these two lengths are 2 and 4 s respectively. Since the droplets have to cool down to the chamber temperature after injection, the residence time at the desired temperature is shorter. In the case of the lowest investigated temperature of 235 K it is reduced to 1.4 and 3.4 s for chamber lengths of 40 and 80 cm. At the end of the chamber, a Condensation Particle Counter (CPC, TSI 3772) is connected to measure the concentration of the aerosol particles. In order to discriminate between water droplets and ice crystals, an in-house developed Ice Optical Detector (IODE) (Nicolet et al., 2010) was used. In order to avoid the presence of two droplets simultaneously in the laser beam, a new laser was installed (402 nm, Schaefter + Kirchhoff laser Makroliniengenerator13 LTM) providing a rectangular instead of a circular laser beam. The fall velocity of the droplets is 0.210 m s^{-1} calculated as the sum of the terminal velocity of the droplets (0.1860 m s^{-1}) and the

ACPD
15, 12167–12212, 2015

flow velocity at the center of the chamber (0.024 ms^{-1}) using the formula by Rogers (1988) neglecting the temperature gradient term. The Reynolds number of the air flow is calculated to be 12 and the droplets Reynolds numbers are about 0.65 which ensures that the chamber flow is not turbulent. With such conditions inside the chamber, the relative humidity around the column of droplets will increase only slightly due to evaporation of droplets. Our calculations show that this increase is < 1 % and too small to trigger deposition nucleation on the aerosol particles. Stetzer et al. (2008) showed that deposition nucleation on silver iodide particles can take place only when the relative humidity with respect to ice is larger than 105 %.

3.2 Aerosol preparation

Silver iodide particles were produced by mixing of 0.1 M potassium iodide and 0.1 M silver nitrate solutions. 10 mL of the potassium iodide solution was diluted with 80 mL distilled water and 10 mL of the silver nitrate solution were added. The AgI precipitate was then decanted to 40 and 60 mL distilled water was added to the solution. From this solution aerosol particles were produced by atomizing. The particles were then dried to RH < 10 % at room temperature. These dried particles passed through a mixing volume to obtain a relatively constant concentration of particles. At the exit of the mixing volume, a cyclone with 1 µm cutoff size was used and the particles were then passed to the Differential Mobility Analyzer (DMA). The particles have a charge of 1e after the size selection by the DMA which was operated at 1 liter outflow and 10 liter sheath flow air. Selected 200 nm diameter particles were passed to the chamber via a concentration control system in order to select a particular concentration of particles. The aerosol concentration was measured at the end of the chamber with a CPC.

3.3 Charge measurement

The droplets obtain a variable number of charges when the stream of droplets is injected from the droplet generator and the charge can be measured with various meth-

ACPD
15, 12167–12212, 2015

ods. We chose to determine the charge by passing the droplet stream through a capacitor consisting of two parallel plates which were connected to a DC voltage supply. The droplet generator was placed exactly at the top edge of the plates. These two plates were kept at 6 mm distance from each other and a DC voltage was applied. Due to the presence of the charge on the droplets, the droplets were either deflected toward the positively or negatively charged plate. Multiple measurements were performed at different times in order to obtain the average charge on the particles. The charge on the droplets varied from 0.16 fC (1000 e) to 80 fC (50 000 e). The charge on the droplet remained the same once the droplet generator was turned on but could shift to a different value when the droplet stream was turned off and turned on again. The mean charge on the droplets was about 65 fC (39 000 e ± 20 000 e).

3.4 Experimental procedure

The collision ice nucleation experiments were conducted at temperatures between 261 and 236 K. Initially the chamber was evacuated for 5 min and then cooled to 258 K. To cover the walls with a thin layer of ice the chamber was filled with distilled water for 10 s and then flushed out. The chamber was again evacuated for 3 min and the detector was mounted. When the desired temperature of the chamber was reached, the droplet generator was turned on and droplets were observed in the detector. This blank experiment without aerosol particles was performed at each temperature in order to ensure that there is no droplet freezing without particles. After the blank experiments, the aerosol flow was turned on and the actual experiment was performed. After completing the experiment for one temperature, the temperature of the chamber was lowered in steps of 2 to 3 K until the homogeneous freezing temperature was reached.

ACPD
15, 12167–12212, 2015

4 Experimental results

Figure 1 shows the frozen fraction of droplets as a function of temperature for the investigated concentrations of the 200 nm silver iodide particles and residence times of 2 s (panel a) and 4 s (panel b). Error bars shown represent an uncertainty in the frozen fraction due to the classification (liquid or ice) uncertainty originating from the measurement errors of the IODE detector (Lüönd et al., 2010). As the chamber temperature was decreased the frozen fraction started to rise and after reaching a certain value it remained constant. The frozen fraction plateau is reached at about 245 K. A frozen fraction of 1 is not reached even for the lowest investigated temperature of 238 K. According to classical nucleation theory, homogeneous nucleation becomes effective only for $T < 238$ K (e.g. Ickes et al., 2014). We assume that for $T < 245$ K heterogeneous freezing on AgI particles is so efficient that each collision of a particle with a droplet leads to the immediate freezing of the droplet (freezing efficiency of 1) and the frozen fraction plateau is reached. For $T > 245$ K, the probability of droplet freezing is < 1, and the collision of a particle with a droplet does not necessarily induce freezing. For $T < 245$ K, frozen fractions increase with increasing particle concentration from 500 to 5000 cm^{-3} without reaching a value of 1 and they are higher for 4 s residence time than for 2 s residence time. This is in accordance with immediate contact freezing once the droplet has collected a particle. This limits the contact freezing by the probability that a droplet actually captures a particle while it is falling through the chamber. If the freezing probability for $T < 245$ K is assumed to be 1, this temperature range can be used to deduce collision efficiencies from our experimental data. We therefore define data points that correspond to unity freezing probability and use them to derive experimental collision efficiencies. These points are indicated by open symbols in black rectangles in Fig. 1. Figure 2, shows the evolution of the frozen fraction as a function of the residence time in the chamber calculated as

$$FF = 1 - e^{-E_{exp} K_{geo} C_{par} t} \quad (19)$$

ACPD
15, 12167–12212, 2015

where K_{geo} is the geometrical area swept out by the droplet per unit time t. C_{par} is the particle concentration and E_{exp} is the collision efficiency that fits to the experimental results best. Since the collision efficiency should be the same for all concentrations and not depend on residence time, E_{exp} was determined by simultaneously minimizing the difference between the mean values of frozen fraction indicated by the symbols in Fig. 2 and the frozen fraction calculated with Eq. (19). This yielded a value of E_{exp} = 0.13 in reasonable agreement with all data points taking experimental uncertainties into account. To show the sensitivity of the frozen fraction to the assumed collision efficiency, curves for E = 0.02 (according to Fig. 6) are also given in Fig. 2 (as dashed lines).

5 Comparison of the different formulations of collision efficiency

To compare the experimentally derived collision efficiency of E = 0.13 with total collision efficiencies calculated with the theoretical expressions of Sect. 2, we will calculate collision efficiencies for an AgI aerosol by water droplets falling through the 80 cm CLINCH chamber which is held at ice saturation at 261 K. Temperature and vapor pressure gradients between the droplet surface and the surrounding are calculated as well as the slow evaporation of the droplet along its path through the chamber in time increments of 0.01 s. Mean collision efficiencies for the whole chamber length are obtained by averaging over the individual 0.01 s increments. In this simulation, the droplet has a diameter of 80 µm when it enters the chamber and shrinks to 79 µm at the end of the chamber. This slow evaporation induces a temperature gradient between the surrounding and the droplet ($T_a - T_s$ = 0.3 K) leading to thermophoresis. AgI particles have a density of 5600 kg m^{-3} and one elemental charge since they passed through a DMA for size selection. Major uncertainties are associated with the charge of the droplets. For the calculations shown in Fig. 3, a charge of 50 000 e of opposite sign to that of the particles was assumed. Figure 3a shows the collision efficiencies of Brownian diffusion, interception and impaction for the formulations P05 described in Sect. 2.2.1 and S83

ACPD
15, 12167–12212, 2015

described in Sect. 2.2.2. The formulations for Brownian diffusion and interception by P05 and S83 show a very similar particle size dependence, but the values using S83 are by about a factor of three higher for E_{Br} and even an order of magnitude higher for E_{int}. While the formulations of P05 are derived theoretically from a resolved flow field, S83 used dimensional analysis coupled with experimental results. Although the formulation of P05 takes the increased collision efficiency for a flow around a liquid droplet compared with a flow around a solid sphere explicitly into account, it yields lower collision efficiencies than the one by S83. The formulation of S83 crucially depends on the accuracy of the experiments forming the basis for the dimensional analysis. E_{imp} using S83 drops off to zero for a particle diameter $d_p < 2\,\mu m$ because of the critical Stokes number in the formulation of impaction below which the impaction of particles on droplets is zero. For particles smaller than 0.1 µm, Brownian diffusion is the most dominant mechanism and for particles above 1 µm diameter, impaction dominates for the formulation of P05. For the 200 nm particles used in our experiments the collision efficiency by Brownian diffusion is by more than an order of magnitude more efficient than interception and impaction.

Figure 3b shows the collision efficiencies due to individual contributions for thermophoresis and electrophoresis. Diffusiophoresis results in a repulsive force rendering the collision efficiency negative for the formulation of A06 ($\approx -10^{-4}$) and too small to be represented in Fig. 3 using W78 ($\approx 10^{-28}$). While collision efficiencies by electrophoresis are almost identical, considerable differences for thermophoresis in particle size dependence can be found comparing the formulations A06 and W78. A06 predicts a decrease of collision efficiency for increasing particle size whereas W78 shows hardly any dependence on aerosol particle diameter. The expression by W78 is formulated for the slip regime ($Kn < 0.1$) and applies to larger particles (Leong et al., 1982). The expression of A06 applies to the free molecular regime ($Kn > 10$) and small particles (Slinn and Hales, 1971). Electrophoresis contributes the most for the smallest of the aerosol particles i.e. between the range of 1 nm to 0.1 µm diameter.

ACPD
15, 12167–12212, 2015

5.1 Temperature dependence of thermophoretic collision efficiency

Figure 4a shows the dependence of the collision efficiency due to thermophoresis for T = 263, 248 and 233 K, keeping the other parameters the same as used for Fig. 3. As the temperature decreases the effect of thermophoresis also decreases because the evaporation rate of the droplet decreases and therefore also the temperature gradient decreases. On the other hand, the collision efficiency by thermophoresis is also influenced by the decreasing relative humidity with decreasing temperature from 90.6 % at 263 K to 78.2 % at 248 K and finally to 67.8 % at 233 K because the chamber is kept at ice saturation conditions. To take apart the influence of temperature and relative humidity, Fig. 4b shows the dependence of thermophoresis on temperature keeping the environmental relative humidity with respect to water at 90 %. In addition to that, curves T = 298 K are also shown as dash dotted lines for a better comparison with other studies. The temperature dependence of W78 is much stronger than the one of A06. Since for our experimental settings, diffusiophoresis results in a repulsive force rendering the collision efficiency negative or zero, we do not show here the temperature dependence of diffusiophoresis. The combined description of thermophoretic and diffusiophoretic forces indicate that for our experimental conditions of evaporating droplets in the presence of rather small aerosol particles, thermophoresis should exceed diffusiophoresis (Slinn and Hales, 1971). However, disagreement still exists between experiments and model predictions concerning the prevalent forces as a function of particle radius (Santachiara et al., 2012; Prodi et al., 2014).

5.2 Charge dependence of electrophoresis

Figure 5 shows the droplet charge dependence of electroscavenging for the formulations of A06 and W78. Calculations are shown for droplet charges of 5000, 10 000, and 50 000 e and a particle charge of 1 e. All other parameters are the same as for Fig. 3. Charges on droplets and particles are of opposite sign. Both formulations show the same charge and particle size dependence with a strong increase of collision ef-

ACPD
15, 12167–12212, 2015

ficiencies with increasing droplet charge and decreasing particle size. If the charges of droplets and particles were of the same sign, particles would be repulsed from the droplets and the collision efficiency would be effectively zero, since the formulations of A06 and W78 both assume point charges located in the middle of the particles and droplets and do not take into account image charge effects. When aerosol particles come close enough to water droplets, image charges on the conducting droplets can lead to attraction even if the charges on the particle and on the droplet are of the same sign (Tinsley et al., 2000). When the radial component of the flow carries the particle towards the droplet as fast as the particle is repulsed, then the particle will pass through the distance of maximum repulsion and in most cases collide with the droplet, as the image forces increase very rapidly at close distance. Tinsley et al. (2000) show in their Fig. 5c and d, that for particles with diameters > 500 nm and charges of 5–500 e electroscavenging by droplets with 84 µm diameter and a charge of 500 e does not depend on whether the charges of droplets and particles are of the same or opposite sign. Particles with diameters < 200 nm are strongly repulsed from the droplets when their charge is of the same sign as the droplet charge and strongly attracted when the charges are of opposite sign. For particles with diameters of 200 nm, collision efficiencies are by a factor of 2 larger in case of opposite sign than in case of same sign. Also for our experimental situation image charges will diminish the difference between electroscavenging between particles and droplets of like and opposite charges. However, the effect might be smaller because the AgI particles carry only one elementary charge resulting in a smaller image force compared to the situation shown in Tinsley et al. (2000), and the droplets are highly charged, increasing the radius of repulsion that has to be overcome until attractive image forces set in.

5.3 The total collision efficiency E_{Tot}

Figure 6 shows the total collision efficiency for different combinations of the theoretical formulations for the same experimental conditions as in Fig. 3. All combinations of collision efficiencies are dominated by electrophoresis for particle diameters < 100 nm and

ACPD
15, 12167–12212, 2015

by impaction for diameters > 2 µm. In this range Brownian diffusion, electrophoresis and thermophoresis contribute significantly to the total collision efficiency. For 200 nm particles, the total collision efficiency is lowest (0.01) for the combination P05 and A06 and highest (0.02) for the combination S83 and W78. In our approach total collision efficiencies are obtained by adding up collision efficiencies of the different processes with values ≥ 0. Negative collision efficiencies were not considered since they lack physical meaning. In trajectory calculations (Tinsley, 2010; Tinsley and Leddon, 2013) the simultaneous action of the different forces on the particle can be investigated. These calculations show that e.g. for small particles, the total collision efficiency can be lower than the one by Brownian diffusion alone when Brownian diffusion is diverted by repulsion of particles carrying charges of the same sign as the droplet (Tinsley et al., 2006).

6 Comparison with previous experimental work

A direct comparison of our experimental results with other measurements of collision efficiencies is not possible because collision efficiency is sensitive to many parameters, which are only partly the same in different experiments. Important parameters that determine the collision efficiency are droplet and particle sizes, charges on droplets and particles, relative humidity and temperature. Laboratory studies summarized by Wang and Pruppacher (1977) and Ladino et al. (2011b) have all been performed at or close to room temperature. In a critical review, Wang and Pruppacher (1977) criticize most older studies for insufficient control of relative humidity, insufficient control or knowledge of charges on droplets and particles, and the use of large droplets so that the terminal velocity is not reached during the experiment. In the following, the relevant studies to compare with our data are summarized. Lai et al. (1978) investigated collection efficiency of AgCl aerosol particles by freely falling water droplets in nitrogen. For 300, 500, and 900 nm diameter particles scavenged by 1.24 mm diameter droplets, they measured collection efficiencies of 0.107, 0.016 and 0.045, respectively. These results

ACPD
15, 12167–12212, 2015

are in agreement with ours considering the larger particle and droplet sizes employed by Lai et al. (1978). When 1.24 mm diameter droplets were charged with surface charge densities of -0.7×10^{10} to -3.0×10^{10} C cm^{-2} and $+0.8 \times 10^{10}$ to $+3.1 \times 10^{10}$ C cm^{-2}, the collection efficiency for 480 nm diameter particles increased from 0.017 to 0.023–0.067 irrespective of the sign of the charge. This increase illustrates the effect of image charge that is also expected to influence our collision efficiencies. Byrne and Jennings (1993) and Barlow and Latham (1983) obtained collision efficiencies in reasonable agreement with Lai et al. (1978) for similar experimental conditions. Radke et al. (1980) performed airborne measurements of aerosol size distributions before and after rain or snow showers in aged air masses and found good agreement with theoretical calculations for particles ≥ 1 µm in diameter, where inertial impaction dominates scavenging. For the submicron aerosol particles the Greenfield gap was narrower than predicted by theory. Measured scavenging collection efficiencies ranged typically from 0.1–0.7 for 200 nm diameter particles which is in general agreement with our results, and dropped to < 0.05 in the size range 400–1000 nm. Beard (1974) determined collection efficiencies of uncharged 700–900 nm diameter particles with 0.40–0.85 mm diameter droplets with charges of 10^{-5}, 10^{-4}, and 10^{-3} esu (1–100 fC) at 99 % RH and a temperature of 24 °C. They found increasing collection efficiencies with increasing droplet charge of 0.5×10^{-4}–3.7×10^{-4} for 10^{-5} esu, 2.3×10^{-4}–11.6×10^{-4} for 10^{-4} esu, and 12.2×10^{-4}–16.1×10^{-4} for 10^{-3} esu, illustrating again the influence of image charge. Their considerably lower values compared with ours can be partly ascribed to the larger particle and droplet sizes and partly to the absence of phoretic forces. The increase of collection efficiency due to phoretic forces can be seen comparing with the results from Lai et al. (1978) performed at low RH, which are two orders of magnitude larger for similar particle and droplet sizes. Wang and Pruppacher (1977) determined collection efficiencies for 500 nm diameter indium acetylacetonate particles collected by water droplets at 23 % RH and 22 °C. They observed for 340 µm diameter droplets with charges of 1.2×10^{-3} esu (15 e) a collection efficiency of 1.8×10^{-2}. The lower value compared with ours can be explained by the larger particle and droplet size and the lower charge

ACPD
15, 12167–12212, 2015

in the experiment of Wang and Pruppacher (1977). Ladino et al. (2011b) determined collision efficiencies for aerosol particles scavenged by cloud droplets in CLINCH using 26 µm diameter droplets. They exposed freely falling water droplets at 298 K and 90 % RH to an aerosol consisting of lithium metaborate particles with diameters between 0.1 and 0.66 µm and observed collision efficiencies between $E = 0.08–1.75$. $E_{tot} > 1$ are obtained because of the high efficiency of Brownian diffusion for small particles. Figure 7 shows that their experimental results are in general agreement with the theoretical predictions. Ardon-Dryer et al. (2015) determined collision efficiencies between Polystyrene Latex Spheres (PSL) with radii from 0.125–0.475 nm and 43 µm diameter droplets charged with 400 ± 40 e. Collision efficiencies ranged from 5.7×10^{-3} to 8.6×10^{-3} for RH = 15 % and from 6.4×10^{-3} to 2.2×10^{-2} at 88 % RH. These values are lower than the ones reached in this study which may be explained by the lower charge on the PSL spheres.

7 Discussion

7.1 Discrepancies between theoretical and experimentally derived collision efficiencies

The experimentally derived collision efficiencies are almost one order of magnitude higher than the theoretical ones. It is unlikely that the experimentally derived ones are by this amount too high. The assumption that every collision leads to droplet freezing can only result in too high collision efficiencies. A conceivable process that would result in an overestimation of the collision efficiency could be that droplet freezing would influence the velocity of the droplets in such a way that frozen droplets collide with liquid ones. However, considering the sequence of frozen and liquid droplets, such a bias does not seem to exists. Brownian diffusion is the main collision mechanism for small particles in the absence of charges and one of the dominating contributions to the total collision efficiencies for the 200 nm diameter particles investigated in this

ACPD
15, 12167–12212, 2015

study. The formulation of S83 predicts higher collision efficiencies than the one of P05 for Brownian diffusion and combinations with S83 for total collision efficiencies yield higher values. However, it is unlikely that uncertainties in the theoretical formulations of this process can account for the total discrepancy between experimentally derived and calculated collision efficiencies. Contributions of impaction and interception to total collision efficiencies are more than one order of magnitude lower than the one of Brownian diffusion and therefore uncertainties in these formulations are not likely to fill the gap between experimentally derived and calculated collision efficiencies. The assumption that the charge on the droplet is 50 000 e and of opposite sign to the one on the particles results in the highest expected value for collision efficiencies due to electric force. Accounting for image forces would only increase collision efficiencies in the case of same charges on particles and droplets. The processes with the highest uncertainties are the ones arising from thermophoretic and diffusiophoretic forces. While diffusiophoresis leads to a repulsive force and does not contribute to the total collision efficiencies under our experimental conditions of evaporating droplets, thermophoresis is attractive and a dominating contribution. In the combined treatment of electrical, thermophoretic and diffusiophoretic forces, collection efficiencies can be lower than when efficiencies are treated separately and added up. In trajectory calculations (Zhou et al., 2009) Brownian motion, electrical and phoretic processes are treated together. Since the diffusiophoretic force of an evaporating droplet is repulsive it can counteract attraction by thermophoresis and Brownian motion. A study on the simultaneous effect of phoretic processes performed by Slinn and Hales (1971) showed that thermophoresis dominates diffusiophoresis for evaporating droplets in quasi-steady state conditions for vapor diffusion and heat conduction. Similarly, the same charges on particles and droplets will divert particles away from the droplets at distances where mirror charges are too weak to lead to attraction and decrease the collision efficiency (Tinsley et al., 2000). For the calculation of collision efficiencies spherical particle shapes have been assumed. This assumption is valid for liquid or glassy particles but not for solid ones, which have complex morphology with significant deviations from sphericity. The drag

ACPD
15, 12167–12212, 2015

on a nonspherical particle depends on its orientation, which in turn is affected by shear in the flow field. Leong et al. (1985) estimated in a theoretical study the effects of oblate and prolate particle rotation in shear flow and shape dependency of the thermophoretic force of evaporating 30 µm radius droplets. The results indicate that the orientation effects of the shear flow will tend to decrease the thermophoretic force on the particle toward the drop surface in the size regime where phoresis dominates beacuse the non spherical particle aligns along the streamlines and the velocity component of the phorestic force is minimized. Foss et al. (1989) investigated the collection of uncharged prolate spheroidal aerosol particles by 30 µm radius collector droplets. They found that such particles can be captured on the downstream side of the collector in the absence of attractive forces in contrast to the case of spherical particles. In the case of prolate spheroidal aerosol particles collected by charged 30 µm radius droplets, the collision efficiencies for particles having large aspect ratios are significantly lower than those for spherical particles when the Coulomb force is dominant. These studies indicate that deviations from particle sphericity rather decrease collision efficiencies for the experimental conditions of our study and cannot account for the discrepancy between measured and calculated collision efficiencies. The largest uncertainties are associated with the theoretical description of phoretic processes at low temperatures. It might be necessary to re-assess these to obtain expressions that are in better agreement with experiments.

7.2 Implications for contact freezing

The efficiency of contact freezing depends on the efficiency of the collision process and the ability of the particle to act as INP. The most important heterogeneous ice nuclei identified in the atmosphere so far are mineral dusts. Size distributions of mineral dusts depend on the age of the air mass because larger particles are removed by gravitational settling. Mineral dust particles cover a large size range from 0.1 to 100 µm (Tegen and Schepanski, 2009; Maring et al., 2003). In the coupled aerosol–climate model ECHAM5-HAM, which was used to investigate heterogeneous contact and immersion

ACPD
15, 12167–12212, 2015

freezing, the mineral dust aerosol is represented by two lognormal modes with mass-median radii of 0.37 and 1.75 µm (Lohmann and Diehl, 2006; Hoose et al., 2008). Small particles collide with droplets mainly due to Brownian diffusion, large ones due to impaction. The predicted number of collisions varies by up to a factor of three for Brownian diffusion and impaction depending on the mathematical formulation that one chooses. Most importantly, in the highly relevant size range for ice nucleation on mineral dusts from 0.5–2 µm, calculated collision efficiencies are strongly reduced when a critical Stokes number is included in the formulation for impaction. In updrafts within clouds a slight supersaturation typically persists, directing particles away from droplets due to thermophoresis which is only partly compensated by attraction due to diffusiophoresis. In downdrafts or when dry air is entrained in clouds, droplet evaporation mostly occurs at cloud top and close to the edges of cumuli, which is the region where first ice in clouds is indeed observed (Young, 1974). Under such conditions, thermophoresis leads to attraction and may contribute significantly to the collision efficiency in the size range 0.1–2 µm. The two formulations for thermophoresis are very different in terms of particle size and temperature dependence. This term has to be re-assessed to improve estimates of contact nucleation in models. In addition electric force act on the particles which may significantly contribute to the overall collision efficiency. Evaporating cloud droplets and aerosol particles released from evaporated droplets from the same region of the cloud are supposed to have like charges (Tinsley and Leddon, 2013). For particles of sizes that act as INP such as mineral dusts, the predominant effect of their charge, irrespective of sign, is an increase in the collision rate due to the short-range electrical image-charge attraction (Tinsley and Leddon, 2013). Layer clouds such as stratocumulus and altostratus are weakly electrified producing droplet charges in the consequent gradients of electric field of the order of 100 e on 20 µm diameter cloud droplets (Zhou et al., 2009). Thunderstorm clouds are strongly electrified (Tinsley and Leddon, 2013) with cloud droplets bearing elementary charges in the range of 10 000–100 000 e. Taking the effect of image charges into account will therefore increase the collision rate of particles with droplets even more. In summary, the collision efficiency

ACPD
15, 12167–12212, 2015

of mineral dust particles with cloud droplets is most probably underpredicted in state of the art aerosol–climate models leading to an underestimation of the relevance of contact nucleation especially in evaporating clouds.

7.3 Implications for atmospheric aerosol scavenging

Impaction scavenging of aerosol particles can occur in cloud and below cloud. Below-cloud scavenging leads to the removal of aerosol particles from the atmosphere between cloud base and ground due to precipitation. In addition to impaction scavenging, in-cloud scavenging includes also contributions from nucleation scavenging (Seinfeld and Pandis, 2006). Aerosol scavenging is usually described by the scavenging coefficient (s^{-1}) defined as the rate of aerosol removal (Chate et al., 2011). In field measurements, the scavenging coefficient is usually calculated from measurements of the change in aerosol size distribution with rainfall (Santachiara et al., 2012). For very small and very large particles, there is mainly an agreement with theoretical studies. However, theoretical parameterizations often underestimate observed scavenging coefficients by one to two orders of magnitude for particles in the 0.2–2 µm diameter range, where collection efficiencies are lowest. Theoretical models predict Brownian diffusion as the dominating scavenging process of particles with diameters < 0.2 µm, and inertial impaction as the main scavenging process for diameters > 2 µm. For aerosol scavenging in the particle diameter range of 0.2–2 µm, contributions from electric and phoretic forces are thought to be important. In the case of thermal equilibrium between the drop and the environment and water vapor evaporation or condensation is the only factor determining the temperature gradient, thermophoresis and diffusiophoresis are supposed to act in opposite directions. However, in rain events, falling raindrops can have a different temperature from that of the ambient air and diffusiophoretic and thermophoretic forces will reinforce each other (Santachiara et al., 2012). Many theoretical studies on scavenging do not take phoretic forces into account, but even those which do are not able to explain the discrepancies between field and observed scavenging coefficients in the Greenfield gap (Santachiara et al., 2012). Most model parameterizations treat

ACPD
15, 12167–12212, 2015

the collision processes separately and either assume that they act in series (Davenport and Peters, 1978) or calculate the total collision efficiency as the sum of individual collision efficiencies (Bae et al., 2009; Andronache et al., 2006). With this approach, the net effect of repulsive and attractive contributions of forces acting on particles cannot be taken into account correctly. Figures 3b and 4 show that the collision efficiency formulations of thermophoresis of W78 and A06 are vastly different. They are derived for large and small particles, respectively, but in most studies applied to the whole simulated particle size range. Moreover, the temperature dependency of the formulations by A06 and W78 are very different indicating also here large uncertainties. From this, it can be concluded that phoretic forces give important contributions to scavenging of aerosol particles in the accumulation mode, but are most probably also the main source of uncertainties in aerosol scavenging predictions.

8 Summary and conclusions

This study uses contact freezing experiments of freely falling 80 µm diameter droplets exposed to an aerosol consisting of 200 nm diameter silver iodide particles. The chamber is kept at ice saturation in the temperature range from 236–261 K leading to slow evaporation of water droplets giving rise to thermophoresis and diffusiophoresis. Droplets and particles bear charges inducing electrophoresis. From the experimental results, a collision efficiency of 0.13 is deduced. It is compared with theoretical formulations which yield values from 0.01–0.02. Brownian diffusion, electrophoresis and thermophoresis contribute the most to these values. Most experimental parameters are well constrained or show little sensitivity with respect to the resulting collision efficencies and can therefore not account for the observed discrepancies. More importantly, comparisons of different theoretical formulations show considerable differences. There are large differences between the formulations for thermophoresis from A06 and W78 regarding size and temperature dependence. Calculated collision efficiencies for impaction in the size range from 0.5–2 µm strongly depend on whether a critical Stokes

ACPD
15, 12167–12212, 2015

number is assumed. The temperature dependence of W78 is much larger than the one of A06. For our experimental conditions, diffusiophoresis results in a repulsive force and does not contribute to the total collision efficiency. It can be expected that in a combined treatment of the forces acting on particles, the calculated total collision efficiency would even be lower. Collision efficiencies are important parameters needed to correctly represent contact freezing and aerosol scavenging in models. Thermophoresis and diffusiophoresis are supposed to give important contributions to scavenging of aerosol particles in the accumulation mode, but are most probably also main sources of uncertainties in aerosol scavenging predictions. For ice nucleation in contact mode an accurate description of collision efficiencies below 273 K are needed. Ice nucleating particles are most probably in the accumulation mode size range. For this size range collection efficiencies are lowest and associated with the largest uncertainties. More experimental data of collision efficiencies especially at low temperatures are needed to validate theoretical formulations. This is to the authors knowledge the first dataset of collision efficiencies acquired below 273 K. More such experiments with different particle diameters are needed to improve the understanding of collision efficiencies.

Author contributions. B. Nagare carried out the experiments and evaluations. B. Nagare and C. Marcolli prepared the manuscript. O. Stetzer supervised the laboratory work and U. Lohmann supervised the work overall.

Acknowledgements. This work was supported by the Swiss National Foundation, project 200020_150169. We thank Luis Ladino for providing data for Fig. 7 and Zamin Kanji, Dan Cziczo, Brian Tinsley, André Welti, Jan Henneberger and Joel Corbin for useful discussions.

References

Andronache, C.: Diffusion and electric charge contributions to below-cloud wet removal of atmospheric ultra-fine aerosol particles, J. Aerosol Sci., 35, 1467–1482, doi:10.1016/j.jaerosci.2004.07.005, 2004. 12177, 12179

ACPD
15, 12167–12212, 2015

Andronache, C., Grönholm, T., Laakso, L., Phillips, V., and Venäläinen, A.: Scavenging of ultrafine particles by rainfall at a boreal site: observations and model estimations, Atmos. Chem. Phys., 6, 4739–4754, doi:10.5194/acp-6-4739-2006, 2006. 12169, 12170, 12172, 12177, 12178, 12179, 12197, 12208, 12209, 12210

Ardon-Dryer, K., Huang, Y.-W., and Cziczo, D. J.: Laboratory studies of collection efficiency of sub-micrometer aerosol particles by cloud droplets on a single droplet basis, Atmos. Chem. Phys. Discuss., 15, 6207–6236, doi:10.5194/acpd-15-6207-2015, 2015. 12192

Bae, S. Y., Jung, C. H., and Kim, Y. P.: Relative contributions of individual phoretic effect in the below-cloud scavenging process, J. Aerosol Sci., 40, 621–632, doi:10.1016/j.jaerosci.2009.03.003, 2009. 12170, 12197

Barlow, A. K. and Latham, J.: A laboratory study of the scavenging of sub-micron aerosol by charged raindrops, Q. J. Roy. Meteor. Soc., 109, 763–770, doi:10.1002/qj.49710946205, 1983. 12191

Beard, K. V.: Experimental and numerical collision efficiencies for submicron particles scavenged by small raindrops, J. Atmos. Sci., 31, 1595–1603, doi:10.1175/1520-0469(1974)031<1595:EANCEF>2.0.CO;2, 1974. 12191

Byrne, M. and Jennings, S.: Scavenging of sub-micrometre aerosol particles by water drops, Atmos. Environ. A-Gen., 27, 2099–2105, doi:10.1016/0960-1686(93)90039-2, 1993. 12191

Chate, D. and Pranesha, T.: Field studies of scavenging of aerosols by rain events, J. Aerosol Sci., 35, 695–706, doi:10.1016/j.jaerosci.2003.09.007, 2004. 12169

Chate, D., Murugavel, P., Ali, K., Tiwari, S., and Beig, G.: Below-cloud rain scavenging of atmospheric aerosols for aerosol deposition models, Atmos. Res., 99, 528–536, doi:10.1016/j.atmosres.2010.12.010, 2011. 12196

Croft, B., Lohmann, U., Martin, R. V., Stier, P., Wurzler, S., Feichter, J., Hoose, C., Heikkilä, U., van Donkelaar, A., and Ferrachat, S.: Influences of in-cloud aerosol scavenging parameterizations on aerosol concentrations and wet deposition in ECHAM5-HAM, Atmos. Chem. Phys., 10, 1511–1543, doi:10.5194/acp-10-1511-2010, 2010. 12170

Davenport, H. and Peters, L. K.: Field studies of atmospheric particulate concentration changes during precipitation, Atmos. Environ., 12, 997–1008, doi:10.1016/0004-6981(78)90344-X, 1978. 12169, 12179, 12197

DeMott, P. J., Prenni, A. J., Liu, X., Kreidenweis, S. M., Petters, M. D., Twohy, C. H., Richardson, M. S., Eidhammer, T., and Rogers, D. C.: Predicting global atmospheric ice nuclei

ACPD
15, 12167–12212, 2015

distributions and their impacts on climate, P. Natl. Acad. Sci. USA, 107, 11217–11222, doi:10.1073/pnas.0910818107, 2010. 12170
Durant, A. J. and Shaw, R. A.: Evaporation freezing by contact nucleation inside-out, Geophys. Res. Lett., 32, L20814, doi:10.1029/2005GL024175, 2005. 12169
Fornea, A. P., Brooks, S. D., Dooley, J. B., and Saha, A.: Heterogeneous freezing of ice on atmospheric aerosols containing ash, soot, and soil, J. Geophys. Res., 114, D13201, doi:10.1029/2009JD011958, 2009. 12169
Foss, J., Frey, M., Schamberger, M., Peters, J., and Leong, K.: Collection of uncharged prolate spheroidal aerosol particles by spherical collectors – I: 2D motion, J. Aerosol Sci., 20, 515–532, doi:10.1016/0021-8502(89)90098-0, 1989. 12194
Greenfield, S. M.: Rain scavenging of radioactive particulate matter from the atmopshere, J. Meteorol., 14, 115–125, doi:10.1175/1520-0469(1957)014<0115:RSORPM>2.0.CO;2, 1957. 12170
Hoose, C., Lohmann, U., Erdin, R., and Tegen, I.: The global influence of dust mineralogical composition on heterogeneous ice nucleation in mixed-phase clouds, Environ. Res. Lett., 3, 025003, doi:10.1088/1748-9326/3/2/025003, 2008. 12195
Ickes, L., Welti, A., Hoose, C., and Lohmann, U.: Classical nucleation theory of homogeneous freezing of water: thermodynamic and kinetic parameters, Phys. Chem. Chem. Phys., 17, 5514–5537, doi:10.1039/C4CP04184D, 2014. 12185
Laakso, L., Grönholm, T., Rannik, Ü., Kosmale, M., Fiedler, V., Vehkamäki, H., and Kulmala, M.: Ultrafine particle scavenging coefficients calculated from 6 years field measurements, Atmos. Environ., 37, 3605–3613, doi:10.1016/S1352-2310(03)00326-1, 2003. 12169
Ladino, L.: Experimental study on collection efficiency and contact freezing of aerosols in a new collision chamber, Ph.D. thesis, ETH, Zuerich, Switzerland, 2011. 12170
Ladino, L., Stetzer, O., Hattendorf, B., Günther, D., Croft, B., and Lohmann, U.: Experimental study of collection efficiencies between submicron aerosols and cloud droplets, J. Atmos. Sci., 68, 1853–1864, doi:10.1175/JAS-D-11-012.1, 2011a. 12170, 12174
Ladino, L., Stetzer, O., Lüönd, F., Welti, A., and Lohmann, U.: Contact freezing experiments of kaolinite particles with cloud droplets, J. Geophys. Res, 116, D22202, doi:10.1029/2011JD015727, 2011b. 12172, 12181, 12190, 12192
Ladino Moreno, L. A., Stetzer, O., and Lohmann, U.: Contact freezing: a review of experimental studies, Atmos. Chem. Phys., 13, 9745–9769, doi:10.5194/acp-13-9745-2013, 2013. 12169

ACPD
15, 12167–12212, 2015

Lai, K.-Y., Dayan, N., and Kerker, M.: Scavenging of aerosol particles by a falling water drop, J. Atmos. Sci., 35, 674–682, doi:10.1175/1520-0469(1978)035<0674:SOAPBA>2.0.CO;2, 1978. 12191

Leong, K. H., Beard, K. V., and Ochs, H. T.: Laboratory measurements of particle capture by evaporating cloud drops, J. Atmos. Sci., 39, 1130–1140, doi:10.1175/1520-0469(1982)039<1130:LMOPCB>2.0.CO;2, 1982. 12169, 12187

Leong, K. H., Beard, K. V., and Stukel, J. J.: The collision of nonspherical aerosol particles with small evaporating water drops, Aerosol Sci. Tech., 4, 445–454, doi:10.1080/02786828508959069, 1985. 12194

Lohmann, U. and Diehl, K.: Sensitivity studies of the importance of dust ice nuclei for the indirect aerosol effect on stratiform mixed-phase clouds, J. Atmos. Sci., 63, 968–982, doi:10.1175/JAS3662.1, 2006. 12195

Lohmann, U. and Hoose, C.: Sensitivity studies of different aerosol indirect effects in mixed-phase clouds, Atmos. Chem. Phys., 9, 8917–8934, doi:10.5194/acp-9-8917-2009, 2009. 12170

Lüönd, F., Stetzer, O., Welti, A., and Lohmann, U.: Experimental study on the ice nucleation ability of size-selected kaolinite particles in the immersion mode, J. Geophys. Res.-Atmos., 115, D14201, doi:10.1029/2009JD012959, 2010. 12185

Maria, S. F. and Russell, L. M.: Organic and inorganic aerosol below-cloud scavenging by suburban New Jersey precipitation, Environ. Sci. Technol., 39, 4793–4800, doi:10.1021/es0491679, , 2005. 12169

Maring, H., Savoie, D. L., Izaguirre, M. A., Custals, L., and Reid, J. S.: Mineral dust aerosol size distribution change during atmospheric transport, J. Geophys. Res., 108, 8592, doi:10.1029/2002JD002536, 2003. 12194

Nicolet, M., Stetzer, O., Lüönd, F., Möhler, O., and Lohmann, U.: Single ice crystal measurements during nucleation experiments with the depolarization detector IODE, Atmos. Chem. Phys., 10, 313–325, doi:10.5194/acp-10-313-2010, 2010. 12182

Park, S. H., Jung, C. H., Jung, K. R., Lee, B. K., and Lee, K. W.: Wet scrubbing of polydisperse aerosols by freely falling droplets, J. Aerosol Sci., 36, 1444–1458, doi:10.1016/j.jaerosci.2005.03.012, 2005. 12169, 12172, 12173, 12208

Prodi, F., Santachiara, G., Belosi, F., Vedernikov, A., and Balapanov, D.: Phoretic forces on aerosol particles surrounding an evaporating droplet in microgravity conditions, Atmos. Res., 142, 40–44, doi:10.1016/j.atmosres.2013.09.001, 2014. 12188

ACPD
15, 12167–12212, 2015

Pruppacher, H. R. and Klett, J. D.: Microphysics of Clouds and Precipitation, Kluwer, Dordrecht, the Netherlands, 1997. 12174, 12176

Radke, L. F., Hobbs, P. V., and Eltgroth, M. W.: Scavenging of aerosol particles by precipitation, J. Appl. Meteorol., 19, 715–722, doi:10.1175/1520-0450(1980)019<0715:SOAPBP>2.0.CO;2, 1980. 12169, 12191

Rogers, D. C.: Development of a continuous flow thermal gradient diffusion chamber for ice nucleation studies, Atmos. Res., 22, 149–181, doi:10.1016/0169-8095(88)90005-1, 1988. 12183

Santachiara, G., Prodi, G., and Belosi, F.: A review of termo- and diffusio-phoresis in the atmospheric aerosol scavenging process. Part 1: Drop scavenging, Atmospheric and Climate Sciences , 2, 148–158, doi:10.4236/acs.2012.22016, 2012. 12188, 12196

Seinfeld, J. H. and Pandis, S. N.: Atmospheric and Chemistry and Physics: from Air Pollution to Climate Change:, John Wiley & Sons, 794–797, 949–954, Inc., 2006. 12170, 12172, 12175, 12196

Slinn, W. G. N.: Precipitation scavenging, in: Atmospheric Sciences and Power Production, chap. 11, Division of Biomedical Environmental Research, US Department of Energy, Washington, D.C., USA, 1983. 12169, 12172, 12175, 12208

Slinn, W. G. N. and Hales, J. M.: A reevaluation of the role of thermophoresis as a mechanism of in- and below-cloud scavenging, J. Atmos. Sci., 28, 1465–1471, doi:10.1175/1520-0469(1971)028<1465:AROTRO>2.0.CO;2, 1971. 12172, 12187, 12188, 12193

Stetzer, O., Baschek, B., Lüönd, F., and Lohmann, U.: The Zurich Ice Nucleation Chamber (ZINC) – a new instrument to investigate atmospheric ice formation, Aerosol Sci. Tech., 42, 64–74, doi:10.1080/02786820701787944, 2008. 12183

Tegen, I. and Schepanski, K.: The global distribution of mineral dust, IOP C. Ser. Earth Env., 7, 012001, doi:10.1088/1755-1307/7/1/012001, 2009. 12194

Tinsley, B. A.: Electric charge modulation of aerosol scavenging in clouds: rate coefficients with Monte Carlo simulation of diffusion, J. Geophys. Res.-Atmos., 115, D23211, doi:10.1029/2010JD014580, 2010. 12180, 12181, 12190

Tinsley, B. A. and Leddon, D. B.: Charge modulation of scavenging in clouds: extension of Monte Carlo simulations and initial parameterization, J. Geophys. Res.-Atmos., 118, 8612–8624, doi:10.1002/jgrd.50618, 2013. 12170, 12190, 12195

Tinsley, B. A., Rohrbaugh, R. P., Hei, M., and Beard, K. V.: Effects of image charges on the scavenging of aerosol particles by cloud droplets and on droplet charging and

ACPD
15, 12167–12212, 2015

possible ice nucleation processes, J. Atmos. Sci., 57, 2118–2134, doi:10.1175/1520-0469(2000)057<2118:EOICOT>2.0.CO;2, 2000. 12189, 12193

Tinsley, B. A., Zhou, L., and Plemmons, A.: Changes in scavenging of particles by droplets due to weak electrification in clouds, Atmos. Res., 79, 266–295, doi:10.1016/j.atmosres.2005.06.004, 2006. 12179, 12180, 12190

Ulmke, H., Wriedt, T., and Bauckhage, K.: Piezoelectric droplet generator for the calibration of particle-sizing instruments, Chem. Eng. Technol., 24, 265–268, doi:10.1002/1521-4125(200103)24:3<265::AID-CEAT265>3.0.CO;2-4, 2001. 12182

Wang, P. K. and Pruppacher, H. R.: An experimental determination of the efficiency with which aerosol particles are collected by water drops in subsaturated air, J. Atmos. Sci., 34, 1664–1669, doi:10.1175/1520-0469(1977)034<1664:AEDOTE>2.0.CO;2, 1977. 12169, 12190, 12191, 12192

Wang, P. K., Grover, S. N., and Pruppacher, H. R.: On the effect of electric charges on the scavenging of aerosol particles by clouds and small raindrops, J. Atmos. Sci., 35, 1735–1743, doi:10.1175/1520-0469(1978)035<1735:OTEOEC>2.0.CO;2, 1978. 12173, 12179, 12180, 12208, 12209, 12210

Wang, X., Zhang, L., and Moran, M. D.: Uncertainty assessment of current size-resolved parameterizations for below-cloud particle scavenging by rain, Atmos. Chem. Phys., 10, 5685–5705, doi:10.5194/acp-10-5685-2010, 2010. 12176, 12177

Young, K. C.: The role of contact nucleation in ice phase initiation in clouds, J. Atmos. Sci., 31, 768–776, doi:10.1175/1520-0469(1974)031<0768:TROCNI>2.0.CO;2, 1974. 12170

Yun, Y. and Penner, J. E.: Global model comparison of heterogeneous ice nucleation parameterizations in mixed phase clouds, J. Geophys. Res.-Atmos., 117, D07203, doi:10.1029/2011JD016506, 2012. 12170

Zhou, L., Tinsley, B. A., and Plemmons, A.: Scavenging in weakly electrified saturated and subsaturated clouds, treating aerosol particles and droplets as conducting spheres, J. Geophys. Res.-Atmos., 114, D18201, doi:10.1029/2008JD011527, 2009. 12193, 12195

ACPD
15, 12167–12212, 2015

Table 1. List of symbols.

B_p	Mobility of particles ($s\,kg^{-1}$)	C_c	Cunningham slip correction (unitless)
C_{Df}	Force constant for ventilated diffusiophoresis ($kg\,m^3\,s^{-2}$)	C_{El}	Force constant for electrophoresis ($kg\,m^3\,s^{-2}$)
C_{Th}	Force constant for ventilated thermophoreis ($kg\,m^3\,s^{-2}$)	C_p	Specific heat capacity of air ($1005\,kJ\,kg^{-1}\,K$)
D_{diff}	Diffusion coefficient of aerosol particles ($m^2\,s^{-1}$)	D_d	Diameter of the droplet (m)
d_p	Diameter of the particle (m)	D_w	Diffusivity of water vapor ($m^2\,s^{-1}$)
E	Collision efficiency	E_{Tot}	Sum of all contributing mechanisms of collision efficiency
E_{Br}	Collision efficiency due to Brownian diffusion	E_{int}	Collision efficiency due to interception
E_{imp}	Collision efficiency due to impaction	E_{Th}	Collision efficiency due to thermophoresis
E_{Df}	Collision efficiency due to diffusiophoresis	E_{El}	Collision efficiency due to electrophoresis
k_a	Thermal conductivity of air ($J\,m^{-1}\,s^{-1}\,K^{-1}$)	k_p	Thermal conductivity of particle ($0.419\,J\,m^{-1}\,s^{-1}\,K^{-1}$)
k_B	Boltzmann constant ($kg\,m^2\,s^2\,K^{-1}$)	P_e	Peclet number
P_r	Prandtl number for air	p_s^0	Saturation vapor pressure at droplet surface
p_a^0	Saturation vapor pressure of environment	R	Diameter ratio between particle and droplet
Re	Reynolds number	Sc	Schmidt number of aerosol particles
Sc_w	Schmidt number for water vapor air	St	Stokes number(S83)
Stk	Stokes number (P05)	St^*	Critical stokes number
T	absolute temperature (k)	T_a	Air temperature (K)
T_c	Air temperature in Celsius	T_s	Temperature of droplet surface (K)
U	Terminal velocity of droplet ($m\,s^{-1}$)	u	Terminal velocity of particle ($m\,s^{-1}$)

ACPD
15, 12167–12212, 2015

Table 2. Greek or Latin letters.

α	Packing density i.e. water volume present in unit volume of air	σ	Viscosity ratio of water to air
μ_a	Dynamic viscocity of air ($kg\,m^{-1}\,s^{-1}$)	μ_a	Viscocity of water at 273 K ($1.787 \times 10^{-3}\,kg\,m^{-1}\,s^{-1}$)
ρ_a	Density of air ($1.293\,kg\,m^{-3}$)	ρ_w	Density of water ($1000\,kg\,m^{-3}$)
ρ_p	Density of aerosol particles (for AgI: $5600\,kg\,m^{-3}$)	τ	Relaxation time (s)
λ_a	Mean free path of air molecules (m)		

ACPD
15, 12167–12212, 2015

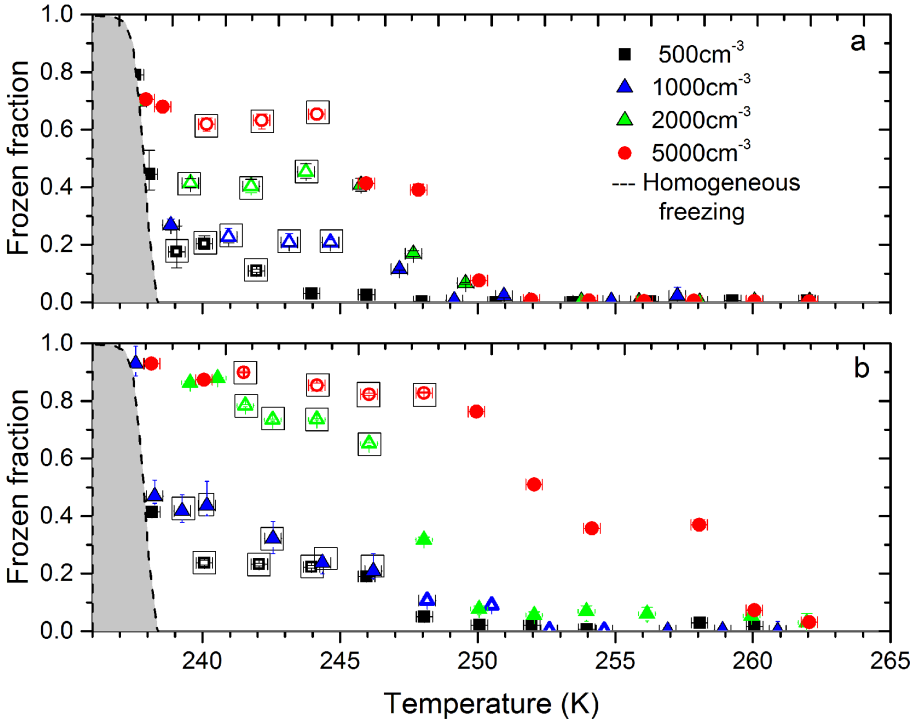

Figure 1. Frozen fraction against chamber temperature for a droplet residence time of 2 s **(a)** and for a droplet residence time of 4 s **(b)** for different concentrations of silver iodide. The dashed line and gray shaded area indicate homogeneous freezing from blank experiments. Open symbols in the black rectangles refer to the experiments used for the calculation of collision efficiencies.

ACPD
15, 12167–12212, 2015

Estimating collision efficiencies from contact freezing experiments

B. Nagare et al.

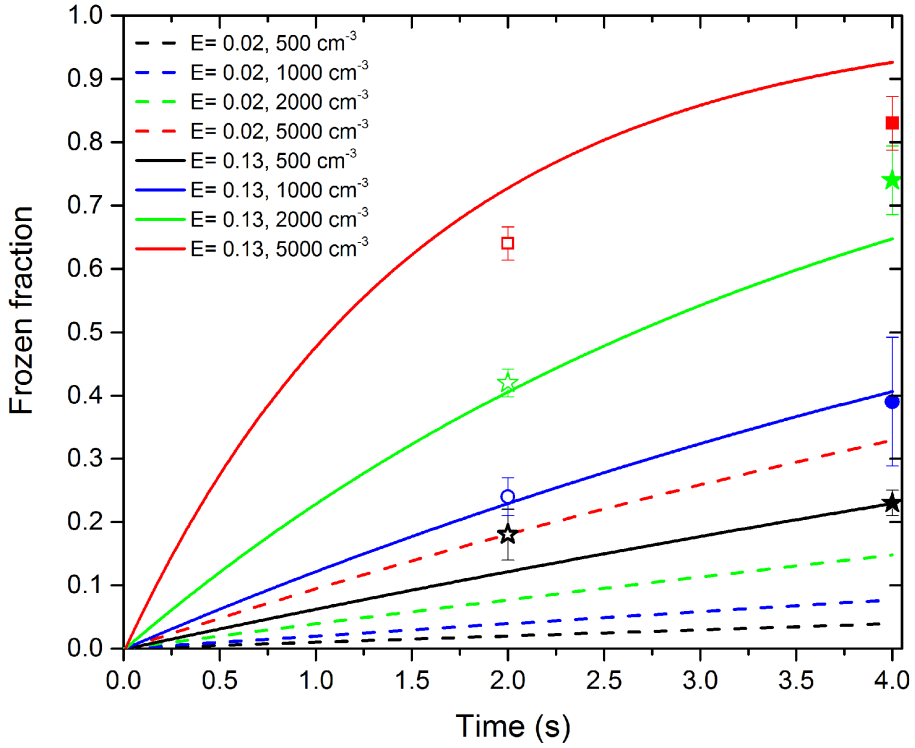

Figure 2. Evolution of the frozen fraction as a function of the residence time in the chamber calculated with Eq. (19) for the different particle concentrations from 500 to 5000 cm^{-3}. Solid lines are calculated assuming a collision efficiency E_{exp} = 0.13, dashed lines for E = 0.02. Symbols and uncertainty bars give the average and SD of the frozen fraction plateau values indicated by open symbols in Fig. 1.

ACPD
15, 12167–12212, 2015

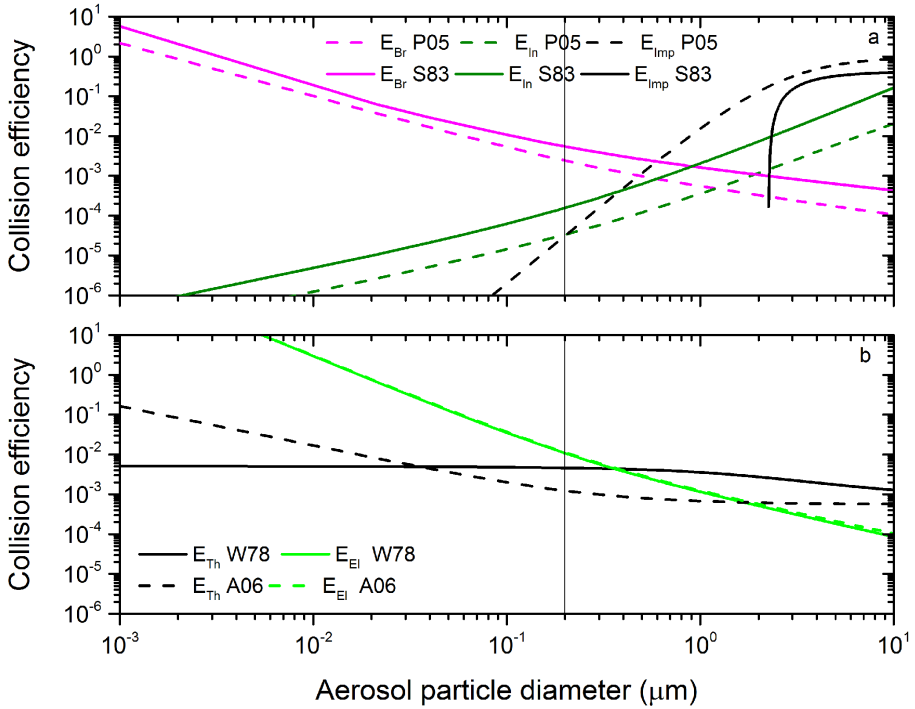

Figure 3. Calculated collision efficiency for a droplet of 80 μm diameter as a function of aerosol particle diameter at a temperature of 261 K and ice saturation. The contributions of Brownian motion, interception and impaction are shown in **(a)** for the formulations by Park et al. (2005) (P05) and Slinn (1983) (S83). The contributions for thermophoresis, diffusiophoresis and electrophoresis are shown in **(b)** for the formulations by Andronache et al. (2006) (A06) and Wang et al. (1978) (W78). The gray vertical line indicates the 200 nm diameter particles used in the experiments.

ACPD
15, 12167–12212, 2015

Estimating collision efficiencies from contact freezing experiments

B. Nagare et al.

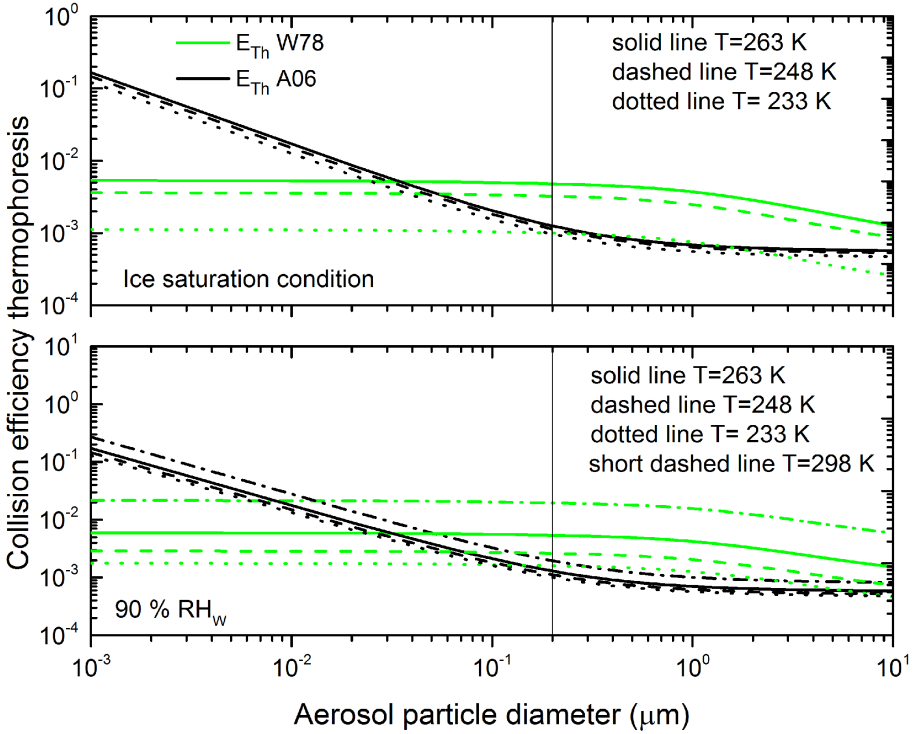

Figure 4. Dependence of thermophoresis on aerosol particle diameter. **(a)** following Andronache et al. (2006) (A06) and Wang et al. (1978) (W78) for a droplet of 80 µm diameter at ice saturation for temperatures of 263, 248 and 233 K. **(b)** shows the dependence of the collision efficiency due to thermophoresis for the same temperatures at 90 % relative humidity with respect to water. The gray vertical line indicates the 200 nm diameter particles used in the experiments.

ACPD
15, 12167–12212, 2015

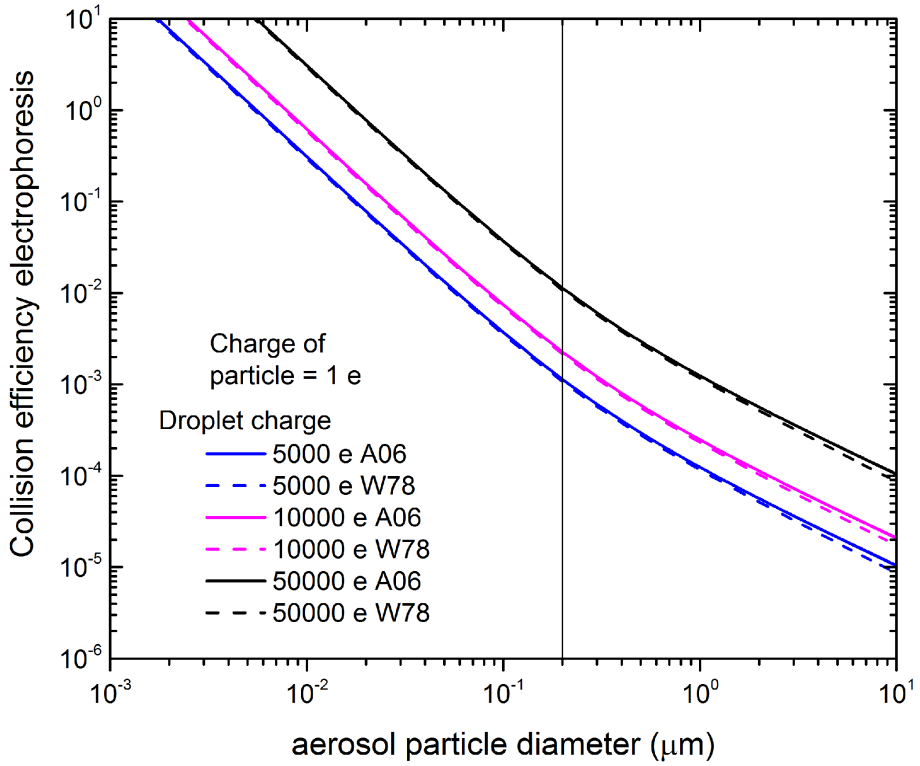

Figure 5. Dependence of electrophoresis on droplet charges for the formulations of Andronache et al. (2006) (A06) and Wang et al. (1978) (W78). The legend indicates the elementary charge on the droplets. The aerosol particles carry one elementary charge. The gray vertical line indicates the particle diameter of our experiments.

ACPD
15, 12167–12212, 2015

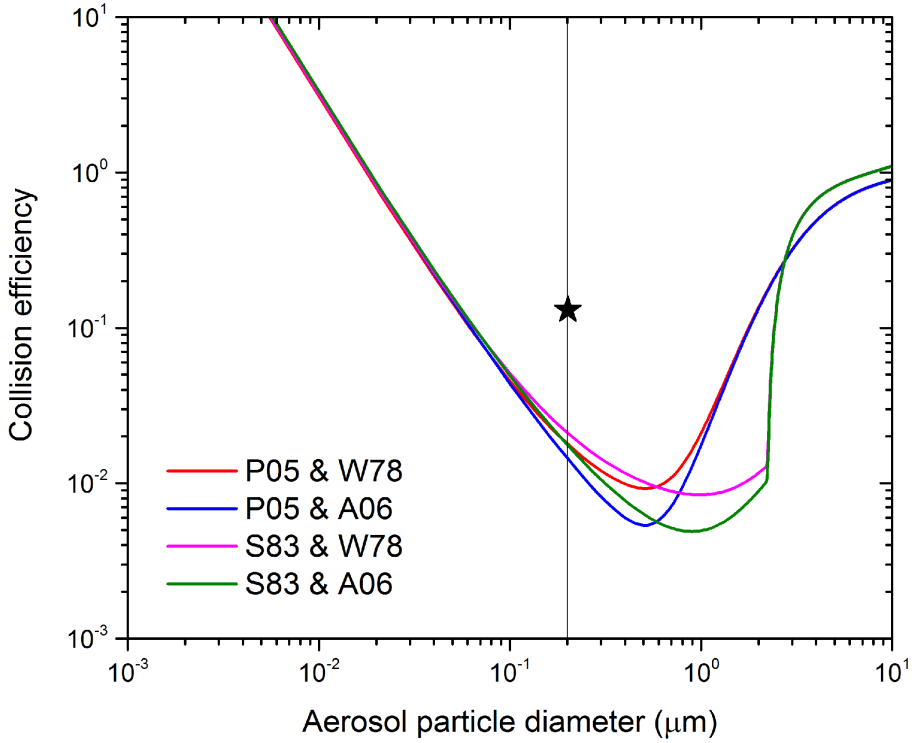

Figure 6. Total collision efficiency for a droplet of 80 μm diameter as a function of aerosol particle diameter at a temperature of 261 K and ice saturation. The total collision efficiency is the sum of all individual contributors. The vertical line indicates the particle size used in our experiment. The experimentally determined collision efficiency for 200 nm silver iodide particles colliding with 80 μm water droplets is shown as black star.

ACPD
15, 12167–12212, 2015

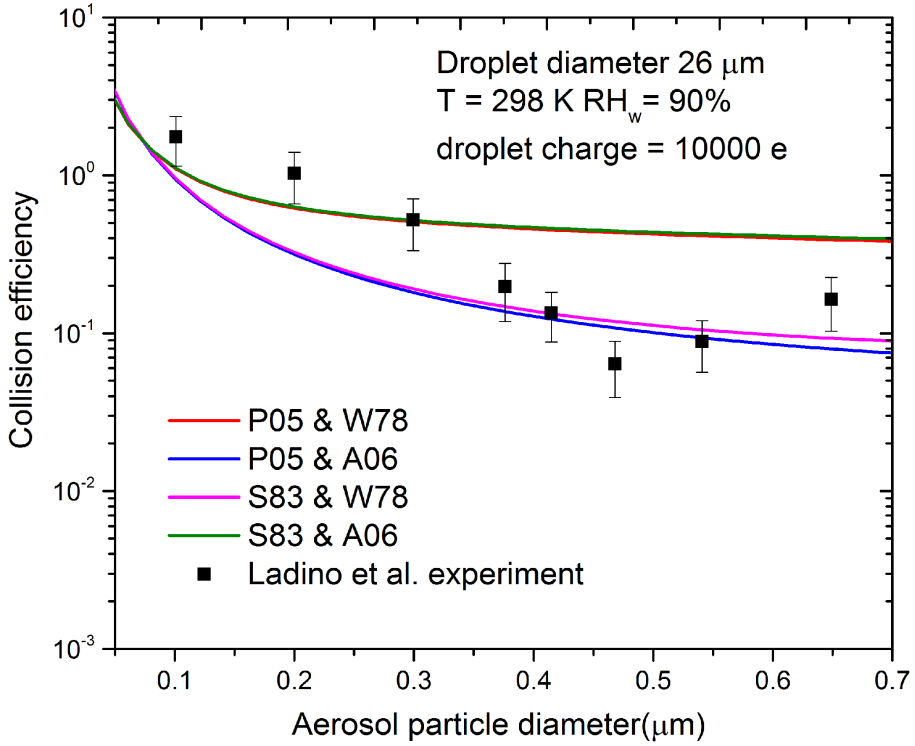

Figure 7. Total collision efficiency for a droplet of 26 μm diameter as a function of aerosol particle diameters at a temperature of 298 K and 90 % relative humidity with respect to water. The black squares indicate the measured collision efficiency.

ACPD
15, 12167–12212, 2015